Bulletin of Geography. Socio-economic Series, No. 62 (2023): 137-151
http://doi.org/10.12775/bgss-2023-0039

BULLETIN OF GEOGRAPHY. SOCIO–ECONOMIC SERIES

journal homepages:
https://apcz.umk.pl/BGSS/index
https://www.bulletinofgeography.umk.pl/

Temporal development of the displacement field of the Ponzano landslide in February 2017

Magdalena Łucka[1, CDFMR], Ryszard Hejmanowski[2, CMR], Wojciech Witkowski[3, CDFM]

[1,2,3]*AGH University of Krakow,* Faculty of Geo-Data Science, Geodesy and Environmental Engineering, Aleja Mickiewicza 30, 30-059 Krakow, Poland; [1]e-mail: magdalena.lucka@agh.edu.pl (*corresponding author*), https://orcid.org/0000-0002-0747-6963; [2]e-mail: hejman@agh.edu.pl, https://orcid.org/0000-0003-1042-4213; [3]e-mail: wwitkow@agh.edu.pl, https://orcid.org/0000-0003-1042-4213

How to cite:
Łucka, M., Hejmanowski, R. & Witkowski, W. (2023). Temporal development of the displacement field of the Ponzano landslide in February 2017. *Bulletin of Geography. Socio-economic Series,* 62(62): 137-151. DOI: http://doi.org/10.12775/bgss-2023-0039

Abstract. The conducted research determined the temporal evolution of the displacement field for the Ponzano landslide case study. The offset-tracking method, so far used mainly for the relatively rapid but uniform displacement of glaciers, was tested for the 2017 study of the Ponzano landslide in Italy. The suitability of the method for high-resolution TerraSAR-X and medium-resolution Sentinel-1 imagery was investigated. The results proved the applicability of the OT method for studying processes with high and variable displacement dynamics. However, for such purposes, high-resolution radar data are crucial. With an uncertainty in the determination of residual displacements of about ±1 m, it was shown that the values of residual displacements occurring up to several days after the main phase of landslide movements are within the range of uncertainty but are determinable. The research conducted in the paper filled a gap in the analysis of the phenomenon just after the main movement phase. It allowed determination of the time and speed of extinction of landslide movements.

Article details:
Received: 09 November 2023
Revised: 21 December 2023
Accepted: 30 December 2023

Key words:
displacement field,
rapid landslide,
offset-tracking,
residual displacements,
satellite imagery

Contents:

1. Introduction

Rapid landslides are caused by various factors, both natural and man-made. Therefore, considering observed climate changes and spreading human activity, they currently affect most parts of the world (Maraun et al., 2022). Global warming influences temperature and precipitation frequency and amount, which are expected to increase the number of shallow landslides and thus enlarge the population affected by landslide risk (Gariano & Guzzetti, 2016; Jakob, 2022). In permafrost areas, melting snow and permafrost are leading to the destabilisation of the soil (Kim et al., 2021). More frequent and intense rainfalls affect the stability of slopes in Europe, South America and south-eastern Asia. The other natural factors that trigger landslides include earthquakes, volcanoes, and river or glacier erosion. On the other hand, human activity, including deforestation, irrigation, producing waste piles, open-pit mining and developing infrastructure in hilly areas, also destabilise slopes and, combined with other factors, might result in a rapid landslide. Due to the severity of the effects of rapid landslides, including the destruction of infrastructure such as roads or houses, the devastation of crops, and even health injuries, the monitoring of landslides, understanding their mechanisms, and further modelling and predicting are crucial (Fell et al., 2007; Hungr, 2007). The increase in landslide hazards in many densely populated regions of the world today poses enormous challenges for scientists and researchers of these phenomena. In particular, the importance of monitoring and early warning of landslides is growing.

A wide variety of techniques are used for landslide monitoring that can be divided into such groups as remote sensing, geodesy, geotechnics, geophysics or hydrology (Auflič et al., 2023). Most of them are in-situ methods, except for the remote-sensing group, which is currently widely used for various purposes such as predicting landslides, susceptibility mapping, monitoring displacements, detection and even modelling or hazard management (Delacourt et al., 2007; Scaioni et al., 2014; Zhao & Lu, 2018; Casagli et al., 2023). In the remote-sensing group, especially useful are SAR (Synthetic Aperture Radar) data as they deliver information regardless of daylight or weather conditions. Thus, they are widely used for landslide monitoring including displacement measurement utilising mainly coherence-based methods (Wasowski & Bovenga, 2014; Raspini et al., 2019; Refice et al., 2019; Ao et al., 2020; Jia et al., 2020; Wang et al., 2022; Huang et al., 2023; Nikolakopoulos et al., 2023). Nevertheless, SAR interferometry (InSAR) cannot be used in all cases because of the coherence loss in dynamically moving areas. Among the remote-sensing monitoring methods, an offset-tracking (OT) technique might be used as an alternative for displacement determination. This OT does not rely on phase information but on searching corresponding intensity patches between two images using cross-correlation, which makes the technique suitable for monitoring rapid movements. So far, the use of this method has been mainly limited to glacial areas, which are characterised by relatively fast movements. However, it has been proven to be particularly useful in landslides (Wang et al., 2016; Cai et al., 2017; Solari et al., 2018; Amitrano et al., 2019; Li et al., 2019). The utility of this method strongly relies on the input image resolution, as the accuracy determined by the method is measured as part of pixel size. The current development of new, high-resolution SAR sensors might improve the possibility of using the OT method to detect smaller and not-extensive movements that occur rapidly. These new possibilities of OT methods became one of the objectives of the study, in terms of one of the most spectacular landslide phenomena of recent years in Europe, the Ponzano landslide (2017). Research into the nature of landslide movements in Ponzano carried out between 2017 and 2020 mainly by Italian scientists (Solari et al., 2018; Calista et al., 2019) might, combined with the new OT-based information about the displacement field, help to find new explanations or add new aspects to the current state of knowledge.

Considering the need to monitor and understand the mechanism of rapid landslides, the research examines the utility of medium (Sentinel-1) and high-resolution (TerraSAR-X) SAR datasets for landslide monitoring and determining optimal processing parameters. It also investigates the scale of movements that can be reliably detected by remote-sensing methods and the temporal development of the displacement field in Ponzano. It allows for determining the displacements in the main phase of movements and post-landslide activity. This study also fills the gap in the monitoring of the Ponzano landslide by deriving the displacement values between the main-phase and the post-landslide *in-situ* monitoring. Therefore, it contributes to a better understanding of the mechanism of the Ponzano landslide.

2. Study area: the Ponzano landslide

The Ponzano landslide is in the central-eastern part of Italy, in the Teramo Province of the Abruzzo region (Fig. 1a; Fig. 1b). It is a very hilly area (Fig. 1d) affected by a significant number of various landslides. The landslide covers an area of ~57 ha (566,759 m^2). It is east-southeast facing and the slope ranges from 4° to up to 20°, with a mean value of 11° (Fig. 1e). The flattest part is located in the centre of the landslide at the south. Some scarps appear mainly in the upper part of the landslide where the steepest slopes are observed and in the eastern part where the slopes range from 15° to 20°. The surface is covered mainly by green areas such as grass, crops and some trees (Fig. 1c). In the upper part of a landslide, there are small groups of buildings and a few roads.

The bedrock in the study area is made of pelitic-arenaceous layers. To the west of the landslide boundaries is a layer of sandstone with thin clay levels with a thickness of 30 to 60 m. The region inside the landslide boundaries consists mainly of clays with sandstone layers and silt and clay with sand, covered by colluvial deposits with a thickness of up to 15 m (Fig. 2). The landslide was activated in the top layer of colluvial deposits and the upper part of the clays (Calista et al., 2019). On February 12, 2017, the region of Ponzano, which is known to be an unstable area, was reactivated mainly due to the intensive rainfall and snowfall that resulted in a large landslide (Solari et al., 2018). It is a complex formation with two components: rotational sliding in the upper part of a landslide and earth flow in the lower part. Before the landslide was reactivated, the area had been stable or slightly moving at a level of 10 to 40 cm total over almost 14 years (Solari et al., 2018). In a phase of major movements, the landslide developed suddenly. In the following five months, it slowed down, but movements totalling almost 75 cm were detected (Allasia et al., 2019). As a result of the movements, local roads and some buildings were seriously damaged, and several dozen inhabitants had to be evacuated.

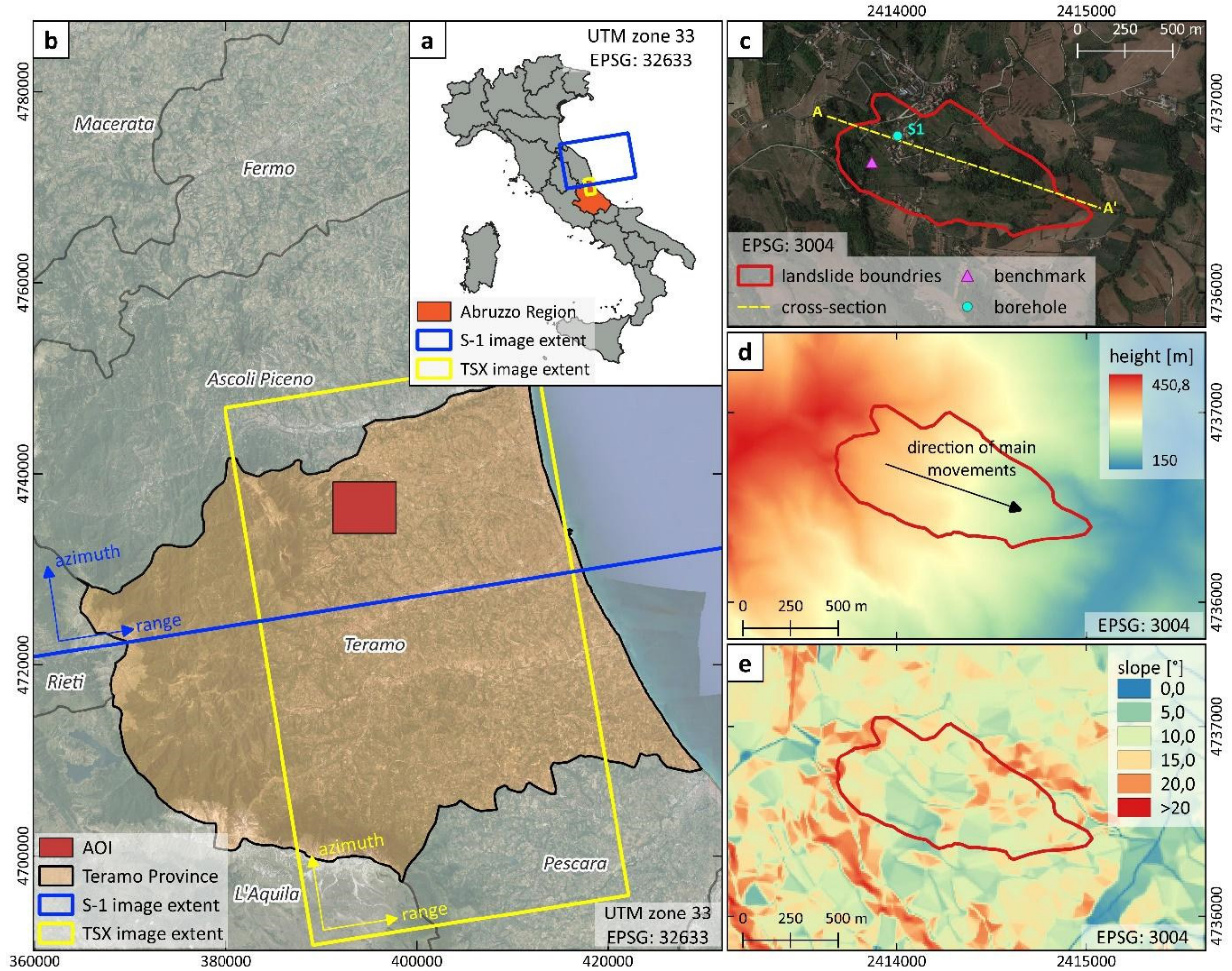

Fig. 1. Location of the research area (a) on the background of the whole country, (b) within Teramo province, (c) land cover and border of landslide, with location of borehole and cross-section, (d) heights derived from TINITALY 10 m DEM (Tarquini et al., 2012) and (e) slope over an AOI

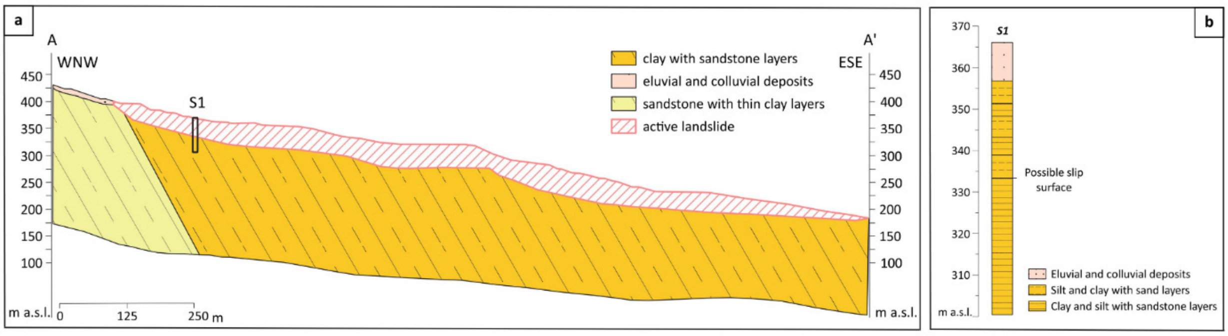

Fig. 2. Cross-section through the Ponzano landslide (a) and geological profile for S1 borehole (b) (modified from Calista et al., 2019)

3. Materials and methods

3.1. Datasets

This study utilises two Sentinel-1 (S-1) and three high-resolution TerraSAR-X (TSX) SAR images. Collected data were used as input for displacement calculations with the OT method. The Single Look Slant Range Complex (SSC) products were used in case of TSX satellite, collected in Stripmap mode and from the ascending track. The polarisation of the data is horizontal (HH). The TSX sensor is classified as high-resolution as the slant range resolution is ~1.2 m. The range and azimuth spacings, which are crucial parameters for the OT method, are 1.36 m and 2.19 m, respectively. The TSX data utilised in this study were acquired in the following way: 1st – just before the landslide occurred; 2nd – immediately after the phase of the main movements, 3rd – after the next 11 days. Those three SAR images were processed in various combinations to obtain displacements in the main phase of the landslide, in a few days after, and in the whole period cumulatively (Table 1). This allows observation of how the landslide movements developed during the analysed period.

From the S-1 mission, the Single Look Complex (SLC) products were used. The data were acquired in the Interferometric Wide (IW) mode and from an ascending track. In this study, only the cross-polarisation (VH) data were utilised. Collected S-1 images have a range spacing of 2.33 m and an azimuth spacing of 13.92 m. It is worth noting that range spacing is ~1.2 times larger compared to TSX data, and in an azimuth direction, the difference is even more significant. The S-1 azimuth spacing is more than six times coarser than the TSX's. To investigate the impact of this difference, two S-1 images were collected covering the phase of main movements (Table 1) to compare results to TSX output. The image pairs with ID 2, ID 3, and ID 4 are referenced in the following text as period 1, period 2, and period 3.

3.2. Offset-tracking

Displacements for both sensors were calculated using the OT method implemented in the Gamma Software. The selected method uses intensity information from SAR data to find corresponding patches between two images from different days. The cross-correlation between image patches is calculated for a selected size of a registration window. The patch with the highest cross-correlation peak is selected as a corresponding image part (Strozzi et al., 2002). In the following steps, the offsets in range and azimuth directions are calculated. The

Table 1. Satellite radar image pairs acquired by the Sentinel-1 and TerraSAR-X mission used in the study

ID	Reference image [dd/mm/yyyy]	Secondary image [dd/mm/yyyy]	Satellite	Temporal Baseline [days]	Perpendicular Baseline [m]	Geometry
1	06/02/2017	18/02/2017	S-1	12	36	ascending
2	10/02/2017	21/02/2017	TSX	11	222	ascending
3	21/02/2017	04/03/2017	TSX	11	136	ascending
4	10/02/2017	04/03/2017	TSX	22	87	ascending

Copernicus 30 m DEM (Digital Elevation Model) was utilised in the preprocessing of the dataset. The OT was employed in two iterations. The first one is to determine the initial offsets, and the second one is to improve the quality of the results. At this step, various sizes of registration windows were investigated to obtain the optimal output. The results were also filtered with a fast spatial filter using a quadratic weighted average. After each iteration, the results were also filtered based on determined thresholds: the minimum and maximum range and azimuth pixel offsets, and the cross-correlation value. The pixel offsets were determined separately for each calculation period, and the minimum cross-correlation value was established at 0.2 to remove displacement values that were determined with the lowest quality. The final results contained the ground range and azimuth displacement values in metres and the magnitude displacements, which were used in further analyses.

3.3. Tests of dimensions of the registration window

To obtain optimal displacement values, calculations for period 1 were performed in various window dimensions for range and azimuth directions. Window sizes from 16 pxl × 16 pxl (range × azimuth dimension) to 256 pxl × 256 pxl were tested. The window dimensions were doubled in each iteration, and near-quadratic windows were also tested (e.g. 256 pxl × 128 pxl). To determine which results are most suitable, analyses of accuracy around the landslide were performed. Two buffers around landslide boundaries, with a 200 m and 1000 m width, were constructed for this purpose (Fig. 3). The landslide area was excluded from the analysis, and the generated buffer zones intersect with each other. All produced rasters of displacements in range and azimuth directions were cropped only to the extent of the buffer zones. Each cropped raster was analysed in terms of the mean value and standard deviation in the selected buffer. It is assumed that the area around the landslide boundaries is stable, so the displacements in the buffer zones should be equal to 0 m. Based on the performed statistical analysis, the optimal window size was selected for further processing of the dataset.

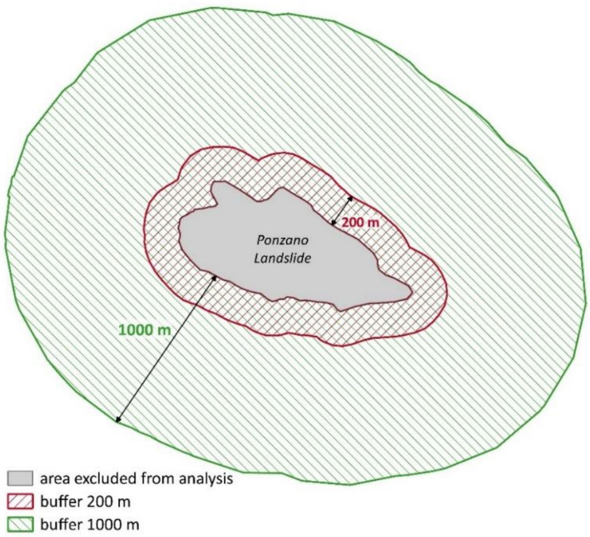

Fig. 3. Schema of buffers used for analysis of results based on various registration windows

3.4. Uncertainty of the results

The final results are presented as the magnitude of the movements (*Mag*), which is determined as a resultant of azimuth (*Az*) and range (*Rg*) displacements. Thus, the uncertainty (standard deviation – σ) of each magnitude raster based on the uncertainties of its components, considered as independent variables might be defined as follows:

$$\sigma_{Mag} = \sqrt{\sigma_{Az}{}^2 + \sigma_{Rg}{}^2} \quad (1)$$

Determination of uncertainty is also possible by analysing displacement in three time periods (from *P1* to *P3*). Residual values of movements (*Res*) determine the accuracy of the results. Their uncertainties might be described in the following way based on the rules of error propagation:

$$Res = Mag_{P3} - (Mag_{P1} + Mag_{P2}) \quad (2)$$

$$\sigma_{res} = \sigma_{Mag}\sqrt{3} \quad (3)$$

Assuming that the uncertainties for all periods are the same, uncertainty can be calculated by equation (3).

4. Results

4.1. Selection of optimal registration window

The first stage of research was to determine the size of the registration window for the Ponzano area. Two TSX acquisitions from 10/02/2017 and 21/02/2017 were used. The mean values of displacements in range and azimuth directions were determined in the buffer zones around the Ponzano landslide. Calculated values with their standard deviations show the accuracy and amount of noise for each registration window size in the 200 m (Fig. 4a) and 1000 m (Fig. 4b) buffers. Increasing window size presents smaller standard deviations and mean values closer to 0 m in both directions. However, the results are strongly smoothed, and the details of the displacement pattern are invisible. Reducing window dimensions allows the detection of more details, but the amount of noise visible on the output is increasing. As an effect, small window dimensions reduce the clarity and reliability of the results. Moreover, in the case of smaller windows, some patterns cannot be observed, and the detection of more significant movements is limited. Considering the trade-off between details and accuracy, the window size of 64 pxl × 64 pxl was selected as an optimal source of information. On the spatial distribution of displacement, areas of more intense and slower movements can be distinguished, providing accurate insight into the displacement

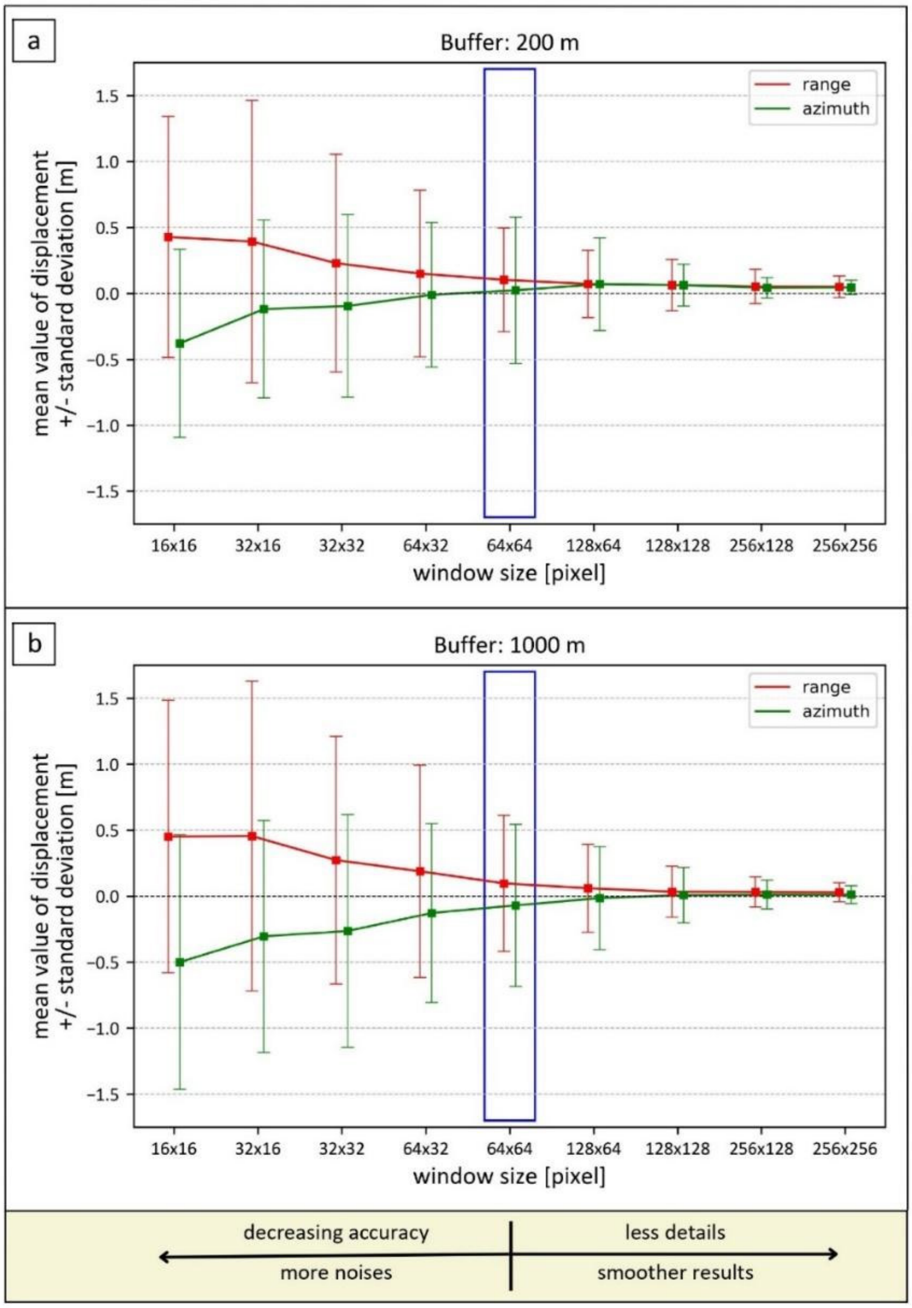

Fig. 4. Relationship between window size and noise amount in (a) 200 m and (b) 1000 m buffer around the landslide

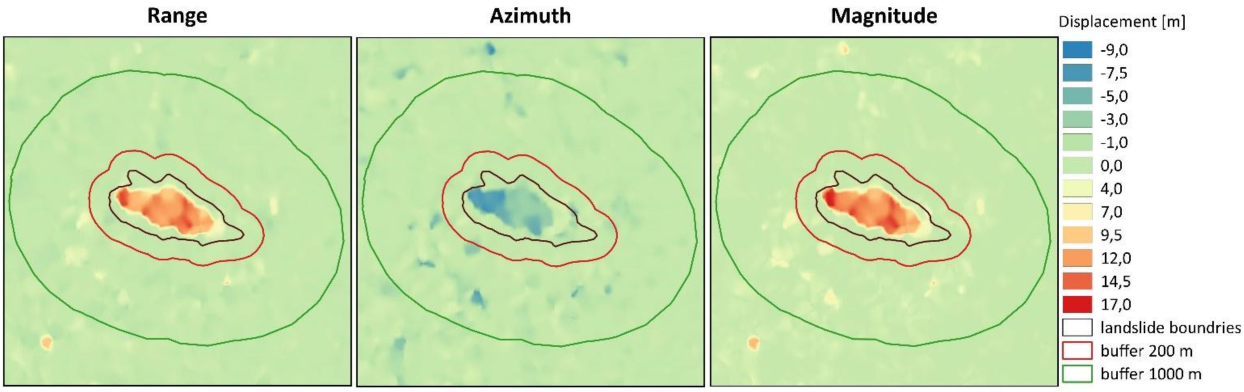

Fig. 5. Spatial distribution of displacements for landslide and selected buffers based on TSX data for period 1 in a 64 pxl × 64 pxl window

field pattern (Fig. 5). A detailed description of the field and its temporal development is provided in Section 4.3. Simultaneously, in the selected buffers of 200 m and 1000 m, the displacement values around 0 m are dominant. The mean values of displacement in both directions and for both buffers are in the range of 2–10 cm. Their standard deviations vary between 0.39 m and 0.61 m. The highest mean value of displacement was 0.10 m for the range direction in the 200 m buffer, and it accounts for 7% of the pixel size of the TSX data. The standard deviations stand in all cases for ~25% of the pixel size in both directions. For the 1000 m buffer, the chart shows slightly higher values of mean and standard deviation. Nevertheless, the same window size presents an acceptable trade-off between details and accuracy. The selected optimal window size was utilised for all periods for TSX data, and, for S-1 data, the corresponding window size was calculated, considering the metric dimensions of the registration box.

4.2. Displacements for the main phase of movements based on S-1 data

Selected in Section 4.1 registration window of 64 pxl × 64 pxl for TSX data corresponds to approximately 90 m × 140 m. To obtain a similar terrain window size for S-1 data, the displacements were calculated in a registration window of 38 pxl × 10 pxl. The results present displacement in range and azimuth directions, as well as magnitude displacement (Fig. 6) over a period covering the main phase of landslide movements. In the range direction, the maximum displacements within the landslide boundaries reach 9 m in the lower part. In the upper part, displacements fluctuate around 8 m. The blurry area of the landslide border can be observed. Nevertheless, the noises observed outside the landslide boundaries also reach high values of several metres, which makes the derived results unreliable, and results present rather random data than the real displacement values. The distribution of displacements in the azimuth direction varies

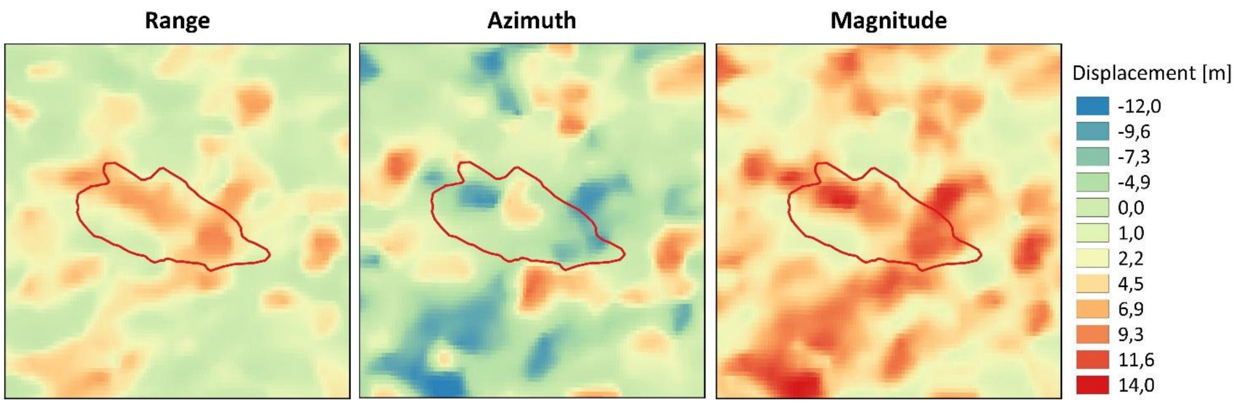

Fig. 6. Displacement values calculated in the period 06/02/2017–18/02/2017 based on Sentinel-1 images in a 38×10 pixel window

between −10 m and +5 m within the marked borders. The highest negative values are observed in the upper part of the landslide, which is consistent with the results from the TSX sensor. The quality of the results in azimuth directions is much lower compared to the range directions. It is caused by such factors as a highly coarser resolution for azimuth direction (almost 14 m) and, at the same time, a smaller scale of movements to be detected. For magnitude directions, the errors and noises from both directions cumulate and, as a result, even outside the landslide boundaries, a large scale of detected movements is observed, which shows the unreliability of the obtained values. Nevertheless, the spatial distribution of the movements within the landslide border is comparable to the TSX results, with the highest peaks at the highest part of the landslide and in the lower part. Simultaneously, all displacement values seem to be slightly underestimated compared to the high-resolution sensor. No further analyses based on S-1 data were conducted for the next periods because of the large amount of noise in the results, even in the detection of large-scale movements.

4.3. Temporal evolution of landslide movements

For the selected optimal window size, the calculations for periods 1 to 3 were performed, revealing the temporal development of the displacement field for the Ponzano landslide. The range, azimuth and magnitude displacements over those three periods were analysed (Fig. 7). In order to analyse only displacements that are the most reliable, the obtained displacement maps were masked by cross-correlation for the patch (ccp) at a value of 0.2. For all periods, the main component of a shift occurred in the range direction. The strong eastern component and negative values for azimuth displacement show that the main flow of the landslide stays in agreement with the general slope direction of the terrain. Although most of the displacement took place in period 1, residual displacement could be observed in the second period. All movements detected by the OT method are within the borders of the Ponzano landslide, according to the database provided by the International Programme on Landslides (IPC).

In period 1, in the range direction, the displacement values are within −0.15–16.8 m. The largest displacement is observed in the upper part of the landslide located in the western part of the AOI. There is a visible cut-off between the stable area and the landslide. Most of the observed displacements exceed the value of 8 m. In the lower part, due to the low ccp values, the precise determination of the displacement pattern is challenging. The most significant azimuth displacement was observed in the upper part of the landslide, with values ranging from ca −6.5 m to −8.0 m. In the central part, the movements reach values around 3 m. In the lower part, displacements gradually decrease. On the magnitude map, three areas with the highest displacement values can be distinguished. The first one is at the top of the landslide with a maximum value of ~16.8 m; the second one is on the southern part, slightly below the first area, with a maximum of 15.5 m; and the last one is at the lower part of the landslide, where the slope is steeper, with a maximum movement equal to 15.1 m.

In period 2, the azimuth displacements vary in the range of ±0.23 m. Considering the standard deviation of the results obtained in Section 4.1, which can be considered the accuracy of the method, the azimuthal results might be considered negligible. Taking into account the aforementioned small values of azimuth shifts, the range displacements are almost identical to the magnitude movements. Displacements are significantly smaller in period 2 than in period 1, suggesting that the main phase of the movements is already finished. Nevertheless, the displacements at a maximum of 1.4 m were still observed in the period of 9 to 20 days after the landslide was triggered, suggesting that the deformation process lasted for the next few weeks. The most significant difference between period 1 and period 2, besides the magnitude of displacements, is the location of the main movements. In period 1, the maximum values were focused in the upper part of the landslide, whereas in period 2, the largest displacements were observed in the lower part of the landslide, especially below the area where the significant slope steepening is observed.

Period 3 comprises displacements that occurred in period 1 and period 2 but were calculated independently. It is visible that the main shift occurred in a range direction, but in the upper part of the landslide the influence of the azimuthal shift is also observed. The range movements reach a maximum of 17 m in the upper part (the steepest part of the landslide) and in the lower part (both in the north and south parts). In the azimuth direction, mainly the upper part of a landslide shows the displacement reaching 7.5 m. In the central part of the AOI, the azimuth displacements vary by around 3 m. The magnitude movements reach peaks in the upper part with a value of 18 m and in the lower, southern part with a maximum of 19.5 m.

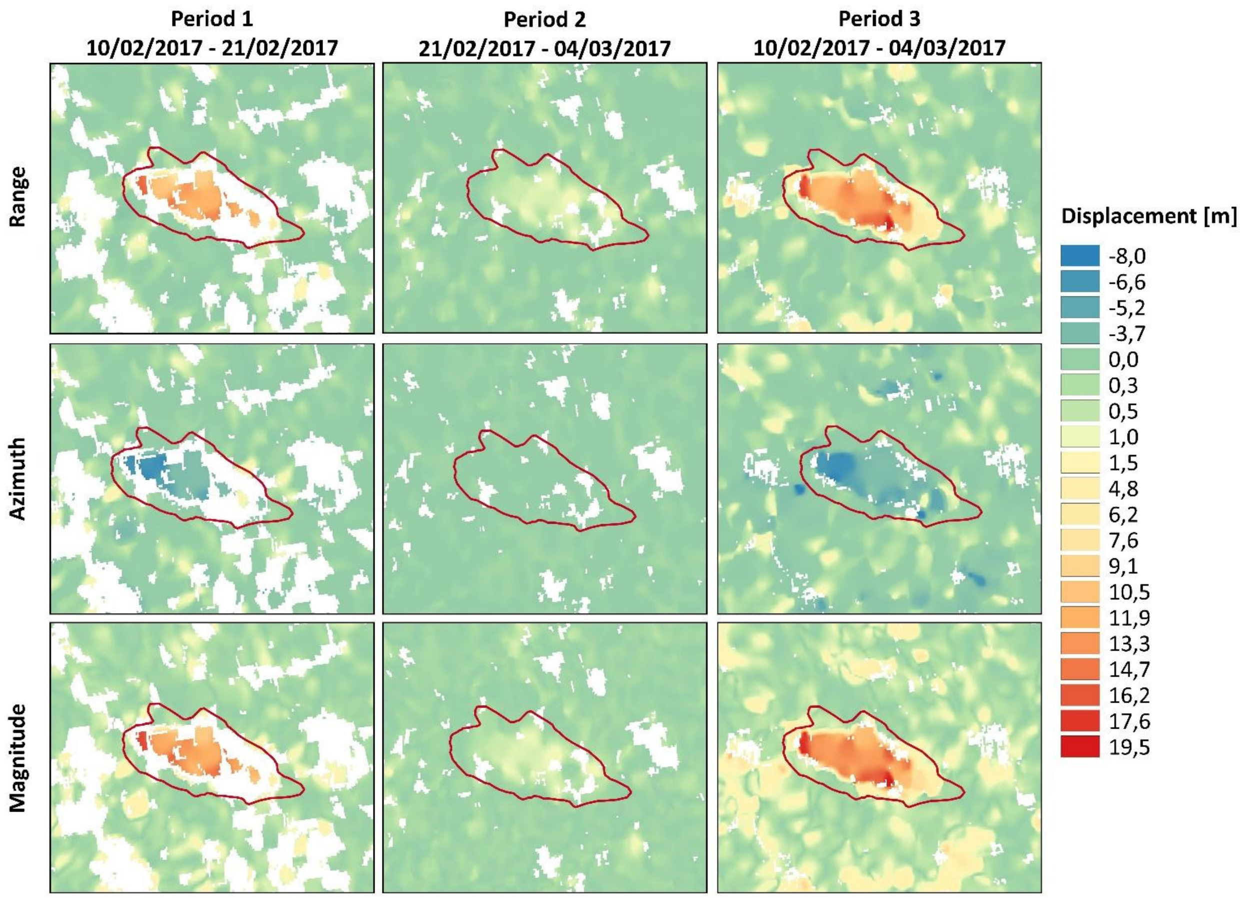

Fig. 7. Displacements derived by TSX data in three analysed periods in range and azimuth directions, and cumulative with masked areas with ccp at 0.2 value

4.4. Comparison between calculations from different temporal baselines

Period 3 should comprise period 1 and period 2 displacements. It is assumed that the difference between cumulative movements from period 1 and period 2 should be equal to those detected in period 3. The magnitude displacements were used for this comparison. The joint part of the masked raster data for all periods was used to determine the discrepancies between period 3 and the summed shorter periods. Those residuals show the inaccuracy of the calculation method, as the input SAR data had identical features for all periods and covered the same dates. The histogram (Fig. 8b) shows that the mean value (μ) of residuals is 0.03. The standard deviation (σ) is equal to 0.94, which means that 68% of all residuals range from −0.91 m to 0.97 m. About 30% of all residuals reach values above 1 m. There are two main areas where the most significant discrepancies are located (Fig. 8a). The first one is in the upper part of the landslide, where the highest displacement values were identified. The second area is in the southern part, near the south border of a landslide. Positive values of the residuals suggest an overestimation of the displacement values over a longer period. Over the major part of the landslide, including the central area, no significant residuals are observed.

Presented in Section 4.1, the analysis showed that for a buffer zone of 200 m, the uncertainty of azimuth and range displacement reached 0.55 m and 0.39 m, respectively. Based on equations from (1) to (4), the standard deviation for magnitude displacements is 0.67 m, and the uncertainty of the calculated residuals is equal to 1.17 m. Figure 8b shows that the standard deviation of residuals is 0.94, which means that unmasked values are within the accuracy of the utilised OT method determined in Section 4.1. Moreover, the applied mask was based on a ccp value, so mostly values that were determined with too low accuracy were removed from the analysis. The presented analysis justifies the use of ccp at a level of 0.2 as a reasonable threshold.

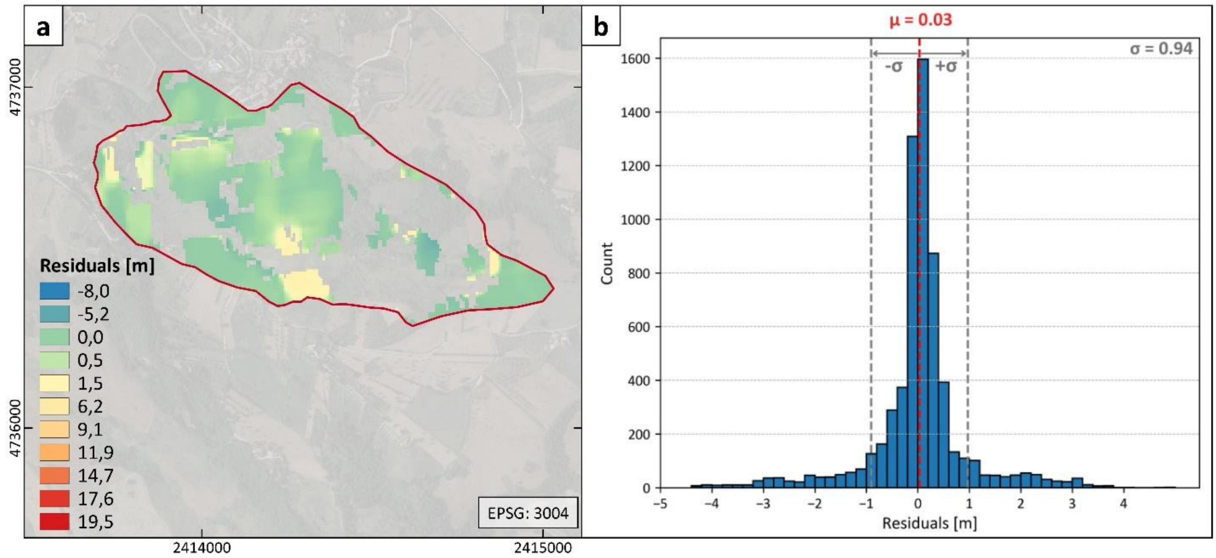

Fig. 8. Residuals between magnitude displacement determined in a long period and cumulative short periods: (a) spatial distribution and (b) histogram of residuals

5. Discussion

The conducted analyses present that even though the OT technique was primarily designed for monitoring glacial areas, it is possible to obtain reliable displacement values by this method for rapid landslides, such as for the Ponzano landslide. Nevertheless, a comparison of the S-1 and TSX datasets revealed that, for a significantly smaller extent of the study area, the medium-resolution S-1 data cannot deliver satisfactory results, in contrast to the TSX imagery. Further investigation about the possibility of applying the OT method in the landslide case study included an analysis of the influence of registration window size on the quality of the results and the accuracy of the obtained displacement maps. The results of the analyses presented in Section 4.1 lead to the conclusion that the size of the optimal window is 64 pxl × 64 pxl. The selected window size reflects the compromise between the visible details in the results and the amount of noise and errors in the background. Similar conclusions are also presented by Wegmüller et al. (2002) and Amitrano, Guida, Di Martino et al. (2019). The former indicates that windows of 64 pxl × 64 pxl or 128 pxl × 128 pxl can be considered a reasonable compromise in the OT method. The latter points out that 64 pxl × 64 pxl windows is the minimum recommended size to obtain reliable values.

Based on the analysis of the displacement values outside the landslide boundaries for the selected optimal window size, the accuracy of the OT method could be established. The mean value for the background ranged from 2 cm to 10 cm, depending on the buffer size and displacement direction. These values correspond to 1% to 7% of pixel size and reflect the mean error of the output displacement maps. Nevertheless, the standard deviation in the background varied from 0.39 m to 0.61 m, which corresponds to ~25% of the pixel size. Those standard deviations might be considered the accuracy of the OT method in this particular case study. In the current state of the art, it is assumed that the OT accuracy might reach 5% of the pixel size (Wegmüller et al., 2002). In the analysed Ponzano landslide case, the obtained accuracy is lower. However, it is worth noting that the calculations of the initial accuracy are performed on the raw results without rejection of the pixels, where cross-correlation values are low. Whereas the analysis of the temporal evolution of the landslide movements in Section 4.3 is performed on the filtered displacement maps, considering only pixels with a ccp higher than 0.2 to provide high-quality data.

In addition, this study reveals the temporal evolution of the displacement pattern for the Ponzano case and fills the gap between existing studies about the landslide evolution in 2017. In this study, for the first time, the pace of the displacements is investigated in detail on a short time scale, allowing us to determine the period in which the dangerous movements might still occur in the landslide area. The existing studies were focused mainly on pre-landslide (Solari et al., 2018) or post-landslide displacements (Allasia et al., 2019). For pre-landslide monitoring, remote-sensing techniques based on SAR imagery were used. Solari et al. (2018) applied the SqueeSAR method and a combination of Sentinel-1 and Radarsat-2 images to provide information about displacement 14 years before the Ponzano landslide was activated in 2017. This study revealed that, since 2003, the cumulative displacement in the analysed area ranged from 10 cm to 40 cm. In the same study, the rapid motion tracking algorithm was used to map displacement in the main phase of landslide movements. These results confirm that the most severe displacement occurred in the crown of the landslide and the displacement pattern confirms observations from Section 4.3. Calista et al. (2019) also presented the displacement map covering the main phase of the landslide movements based on the UAV data, with values reaching even 19 m in the south-easterly direction. The general spatial distribution of the movements and the scale of the detected displacements are consistent with the results of this study. Nevertheless, a direct comparison of displacement values is impossible as the UAV-derived map covers a much longer period. The UAV pre-landslide data are from 2010–13, and the post-landslide data acquisition took place in May 2017 – three months after the landslide was triggered. It can be assumed that the UAV displacement map presents mainly the effect of the February 12 landslide, though some pre- and post-landslide displacements might affect the results presented in Calista et al. (2019). In this study, the cumulative displacements cover only 22 days around the main phase of movement. Nevertheless, the UAV maps provide the most reliable results to compare with the results obtained in this study by the OT methods. The three areas of maximum movement can be observed in both UAV- and OT-derived maps. The areas are consistent, which makes the OT results from the study more reliable. The post-landslide in-situ monitoring carried out by Alasia et al. (2019), shows that until July 2017, some displacements were still observed in Ponzano, reaching a maximum of 72 cm in the upper part of the landslide. Nevertheless, the in-situ monitoring started on February 23, which resulted in a data gap between the date of triggering the landslide and the start of its monitoring. This study aimed to fill this gap and derive information about displacement that occurred right after the main phase of movements slowed down. Such information might be crucial for inhabitants of areas where rapid landslides occur, as it helps to establish the duration of landslide activity and the scale of those residual displacements. A synergy of previous studies and this research provides a more detailed insight into the mechanism of the Ponzano landslide formation, revealing the pace of the displacements for the selected benchmark (Fig. 1c). First, the confidence interval for the OT results was determined. For this purpose, the Student's t-test with the Welch amendment was applied to two groups of the data (period 3 and the sum of period 1 and period 2) around the benchmark. This determined a 95% confidence interval of –0.8 m to +1.5 m. Then, the theoretical function was fitted to the OT results. Due to the rapid growth of displacement values in the initial part of the time series and the more or less constant value for further arguments, it was decided to use one of the functions used in geostatistics, the pentaspherical model (4). Fitting was performed to ensure that the pentaspherical model was within the 95% confidence interval. Utilising the land displacement model, the velocities of land movements (5) were determined.

$$Mag(t) = Mag_0\left(\frac{15}{8}\left(\frac{t}{t_0}\right) - \frac{5}{4}\left(\frac{t}{t_0}\right)^3 + \frac{3}{8}\left(\frac{t}{t_0}\right)^5\right) \quad (4)$$

$$Velocity(t) = \frac{\partial Mag(t)}{\partial t} \quad (5)$$

where: $Mag(t)$ – land displacement in time, t – time, Mag_0 – maximum value of land displacement in t_0 – the moment of occurrence of the maximum land displacement value.

Assuming that `til the end of May, the post-landslide monitoring covered the total displacement value, in the first phase of the movement, consisting of the date of landslide triggering and nine more days, 92% of the total movements were observed by the OT technique. The maximum estimated velocity in this period reached 2.1 m/day at the beginning of the movements (Fig. 9). In this stage, the most significant movements were observed near the landslide corona. This maximum estimated velocity is derived from the availability of TSX imaging dates, so the most likely value of velocity is significantly higher. In the following 11 days observed by the OT method, 4% of the total movement was observed. At this point, the movements were mostly observed in the lower part of the landslide, especially beneath the scarps zone. The maximum estimated velocity at the beginning of this period was 0.56 m/day. It is important to note that in this stage, covering days from 9 to 20 after the triggering of the landslide, residual displacements still reach even 1.4 m. Such a scale of movements means further instability of this region, which might still have negative consequences for inhabitants and infrastructure. In the following days, until the end of May, the post-landslide in-situ monitoring revealed the last 4% of the movements with an average speed of 0.03 m/day. The UAV until the beginning of May showed displacements with a maximum value similar to those from the OT technique; however, the average estimated speed in this case is 0.16 m/day. Considering the uncertainty of the OT data and the errors of the other measurement techniques, it might be concluded that the utilised OT method derived reliable results for the Ponzano landslide based on the TSX data.

Despite the successful application of the OT method in the Ponzano landslide case, the aforementioned technique might not provide reliable results for some rapid landslides. The resolution of the input dataset and the scale of the movements remain limitations of the OT procedure. Section 4.2 points out that S-1 images, which are characterised by coarser resolution compared to TSX, did not provide reliable results even for the main phase of landslide movements. On the other hand, high-resolution datasets enabled captioning movements at the level of a few dozen centimetres. However, such datasets are not as easily accessible as S-1 images. Another limitation is connected with the change in land cover that might accompany a rapid landslide. Too severe changes in land cover result in problems finding corresponding patches on the pair of SAR images. As a result, the application of the OT method in such cases can be challenging. Nonetheless, knowledge gained by studying particular cases like Ponzano might be transferred to similar landslide events.

Rapid landslides have both short- and long-term socio-economic effects on the local population, as well as national consequences. Italy, being one of the European countries with the highest landslide risks, also suffers from the highest economic loss due to landslide activities, estimated at 3.9 billion euros per year (Haque et al., 2016). The expenses affect both public and private properties, and they can be separated into direct costs such as replacing residents or restoring infrastructure and indirect costs such as changing land use cover, which results in, for example, the destruction of agricultural lands (Schuster, 1996). In the event of the Ponzano landslide, 35 residences were evacuated, with many collapsing or sustaining

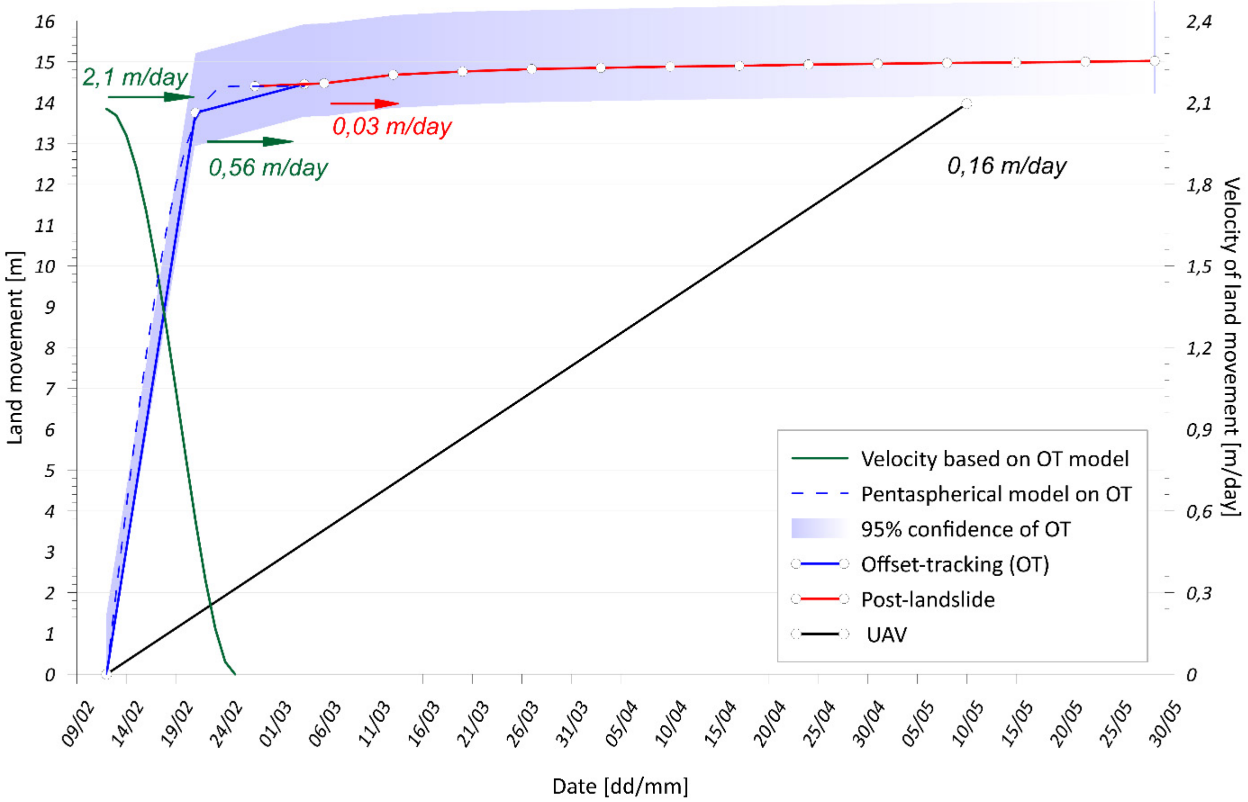

Fig. 9. Time-series for selected benchmark: combined results from this study, UAV and post-landslide monitoring

severe damage. Parts of the roadways at the corona and farther down the landslide were also damaged, resulting in additional costs for road repairs. Most of the damaged regions were used for agricultural reasons, notably olive oil plants. Ground movement and slope destabilisation may result in the loss of growing products. Furthermore, approximately 120 people were forced to leave their homes, either permanently or temporarily. The analyses performed in the study provide more accurate insight into the exact damages caused by the Ponzano landslide, and the technique utilised may also contribute to hazard management in other landslide incidents. Firstly, the OT technique and SAR data analysis can rapidly and safely determine the spatial extent of the disaster, assisting in estimating financial losses due to land changes and mapping buildings in hazard zones that may be harmed. Furthermore, this investigation demonstrated that residual movements could persist in the impacted areas even several days after the landslide was triggered. Consistent monitoring of those movements can aid decision-making and risk assessment by providing information about the safety of the analysed region and the slope's stability. Remote monitoring may also reveal locations that are particularly vulnerable due to significant land movements and should be better safeguarded and closed off to residents. As a result, the OT technique and high-resolution imagery can be utilised to estimate the duration of the dynamic movement phase that threatens people and infrastructure.

6. Conclusions

The current study investigates the feasibility of using the OT technique to detect landslide displacement based on the example of the Ponzano landslide. A key outcome of the studies is new information about the temporal evolution of the displacement field for this landslide. The performed analyses derived information about the scale of movements in a short time scale for the first time, revealing that, in the main phase of the movements, about 92% of all registered displacements were detected. Moreover, during the following 11 days, the residual movements were also observed with their maximum displacement value reaching 1.4 m, which represents the next 4%. The comparison of calculations from various temporal baselines indicates that the values of residual displacements are reliable, as they exceed the uncertainty of the calculations. Those results show for the first time that, after the main phase of the movements, there are still some fading displacements that might threaten the local inhabitants. The last 4% of displacements were observed in the next three months, with a mean velocity of 0.03 m/day. These results showing the pace of an evolving landslide are especially important in the light of increasing intensity of rainfalls and extreme weather conditions that lead to the instability of the ground and in consequence to a higher number of rapid landslides across the world.

Furthermore, the suitability of using medium and high-resolution SAR data was determined. The medium-resolution S-1 SAR data and high-resolution TSX images were used to test the parameters of the OT method and obtain displacement maps for three periods of the landslide's evolution: the main phase of the movement (until 9 days after the landslide was triggered), the phase of residual movements (from 9 to 20 days after triggering), and the longer period covering both previous phases.

The presented results indicate that the OT method, mainly developed for monitoring glacial areas, can also be successfully applied to rapid landslides to quickly and safely map the size of the disaster. Significantly higher quality was obtained for the high-resolution datasets, which enabled the measuring of the main phase of the movements but also of residual displacements that occurred in the several following days. During the testing phase, the optimal registration window size, which is one of the main parameters of the used method, was established at the level of 64 pxl × 64 pxl. For such input data, the uncertainty of results was calculated as ±0.39 m in range and ±0.61 m in azimuth direction, which represent ~25% of the pixel size, considering no filtering by the cross-correlation value.

European countries and other regions in the world will faced an increasing landslide problem in the coming years as a result of climate changes. The impact of these changes on the sense of security of local communities in landslide areas must be addressed. The research presented in this article is a step towards a better understanding of the mechanism of landslides, and thus represents a certain contribution to solving the socio-economic problems of modern societies.

Acknowledgement

The authors acknowledge the European Space Agency (ESA) for providing Sentinel-1 satellite radar images. The presented research is supported by the "Excellence Initiative—Research University" programme for the AGH University of Science and Technology. All high-resolution datasets were accessed via the ESA Third Party Missions programme as a part of the projects: ID 70186 and ID PP0087663.

References

Allasia, P., Baldo, M., Giordan, D., Godone, D., Wrzesniak, A. & Lollino, G. (2019). Near Real Time Monitoring Systems and Periodic Surveys Using a Multi Sensors UAV: The Case of Ponzano Landslide. In IAEG/AEG *Annual Meeting Proceedings*, San Francisco, California, 2018, 1(2): 303–310. Springer International Publishing. DOI: https://doi.org/10.1007/978-3-319-93124-1_37.

Amitrano, D., Guida, R., Dell'Aglio, D., Di Martino, G., Di Martire, D., Iodice, A., Costantini, M., Malvarosa, F. & Minati, F. (2019). Long-Term Satellite Monitoring of the Slumgullion Landslide Using Space-Borne Synthetic Aperture Radar Sub-Pixel Offset Tracking. Remote Sensing, 11(3): 369. DOI: https://doi.org/10.3390/RS11030369.

Amitrano, D., Guida, R., Di Martino, G. & Iodice, A. (2019). Glacier Monitoring Using Frequency Domain Offset Tracking Applied to Sentinel-1 Images: A Product Performance Comparison. *Remote Sensing*, 11(11): 1322. DOI: https://doi.org/10.3390/rs11111322.

Ao, M., Zhang, L., Dong, Y., Su, L., Shi, X., Balz, T. & Liao, M. (2020). Characterizing the evolution life cycle of the Sunkoshi landslide in Nepal with multi-source SAR data. *Scientific Reports*, 10(1): 1–12. DOI: https://doi.org/10.1038/s41598-020-75002-y.

Auflič, M. J., Herrera, G., Mateos, R. M., Poyiadji, E., Quental, L., Severine, B., Peternel, T., Podolszki, L., Calcaterra, S., Kociu, A., Warmuz, B., Jelének, J., Hadjicharalambous, K., Becher, G. P., Dashwood, C., Ondrus, P., Minkevičius, V., Todorović, S., Møller, J.J. & Marturia, J. (2023). Landslide monitoring techniques in the Geological Surveys of Europe. *Landslides*, 20(5): 951–965. DOI: https://doi.org/10.1007/S10346-022-02007-1/FIGURES/7.

Cai, J., Wang, C., Mao, X., Wang, Q., Lu, Z., Li, Z., Tomas, R. & Gloaguen, R. (2017). An Adaptive Offset Tracking Method with SAR Images for Landslide Displacement Monitoring. *Remote Sensing*, 9(8): 830. DOI: https://doi.org/10.3390/RS9080830.

Calista, M., Miccadei, E., Piacentini, T. & Sciarra, N. (2019). Morphostructural, Meteorological and Seismic Factors Controlling Landslides in Weak Rocks: The Case Studies of Castelnuovo and Ponzano (North East Abruzzo, Central Italy). *Geosciences*, 9(3): 122. DOI: https://doi.org/10.3390/GEOSCIENCES9030122.

Casagli, N., Intrieri, E., Tofani, V., Gigli, G. & Raspini, F. (2023). Landslide detection, monitoring and prediction with remote-sensing techniques. Nature Reviews Earth & Environment, 4(1): 51–64. DOI: https://doi.org/10.1038/s43017-022-00373-x.

Delacourt, C., Allemand, P., Berthier, E., Raucoules, D., Casson, B., Grandjean, P., Pambrun, C. & Varel, E. (2007). Remote-sensing techniques for analysing landslide kinematics: a review. *Bulletin de La Société Géologique de France*, 178(2): 89–100. DOI: https://doi.org/10.2113/GSSGFBULL.178.2.89.

Fell, R., Glastonbury, J. & Hunter, G. (2007). Rapid landslides: The importance of understanding mechanisms and rupture surface mechanics. *Quarterly Journal of Engineering Geology and Hydrogeology*, 40(1): 9–27. DOI: https://doi.org/10.1144/1470-9236/06-030.

Gariano, S.L. & Guzzetti, F. (2016). Landslides in a changing climate. *Earth-Science Reviews*, 162: 227–252. DOI: https://doi.org/10.1016/j.earscirev.2016.08.011.

Haque, U., Blum, P., Haque, U. & Blum, P. (2016). Costs and deaths of landslides in Europe. EGU General Assembly, 18, EPSC2016-12758. https://ui.adsabs.harvard.edu/abs/2016EGUGA..1812758H/abstract

Huang, H., Ju, S., Duan, W., Jiang, D., Gao, Z. & Liu, H. (2023). Landslide Monitoring along the Dadu River in Sichuan Based on Sentinel-1 Multi-Temporal InSAR. *Sensors*, 23(7): 3383. DOI: https://doi.org/10.3390/S23073383.

Hungr, O. (2007). Dynamics of rapid landslides. *Progress in Landslide Science*, 47–57. DOI: https://doi.org/10.1007/978-3-540-70965-7_4/COVER.

Jakob, M. (2022). Landslides in a changing climate. In Landslide Hazards, Risks, and Disasters, 505–579. *Elsevier*. DOI: https://doi.org/10.1016/B978-0-12-818464-6.00003-2.

Jia, H., Wang, Y., Ge, D., Deng, Y. & Wang, R. (2020). Improved offset tracking for predisaster deformation monitoring of the 2018 Jinsha River landslide (Tibet, China). *Remote Sensing of Environment*, 247: 111899. DOI: https://doi.org/10.1016/J.RSE.2020.111899.

Kim, H., Lee, J.-H., Park, H.-J. & Heo, J.-H. (2021). Assessment of temporal probability for rainfall-induced landslides based on nonstationary extreme value analysis. Engineering Geology, 294: 106372. DOI: https://doi.org/10.1016/j.enggeo.2021.106372.

Li, M., Zhang, L., Shi, X., Liao, M. & Yang, M. (2019). Monitoring active motion of the Guobu landslide near the Laxiwa Hydropower Station in China by time-series point-like targets offset tracking. *Remote Sensing of Environment,* 221: 80–93. DOI: https://doi.org/10.1016/J.RSE.2018.11.006.

Maraun, D., Knevels, R., Mishra, A. N., Truhetz, H., Bevacqua, E., Proske, H., Zappa, G., Brenning, A., Petschko, H., Schaffer, A., Leopold, P. & Puxley, B.L. (2022). A severe landslide event in the Alpine foreland under possible future climate and land-use changes. *Communications Earth & Environment*, 3(1): 87. DOI: https://doi.org/10.1038/s43247-022-00408-7.

Nikolakopoulos, K. G., Kyriou, A., Koukouvelas, I. K., Tomaras, N. & Lyros, E. (2023). UAV, GNSS, and InSAR Data Analyses for Landslide Monitoring in a Mountainous Village in Western Greece. Remote Sensing, 15(11): 2870. DOI: https://doi.org/10.3390/RS15112870.

Raspini, F., Bianchini, S., Ciampalini, A., Del Soldato, M., Montalti, R., Solari, L., Tofani, V. & Casagli, N. (2019). Persistent Scatterers continuous streaming for landslide monitoring and mapping: the case of the Tuscany region (Italy). *Landslides*, 16(10): 2033–2044. DOI: https://doi.org/10.1007/S10346-019-01249-W/FIGURES/7.

Refice, A., Spalluto, L., Bovenga, F., Fiore, A., Miccoli, M.N., Muzzicato, P., Nitti, D.O., Nutricato, R. & Pasquariello, G. (2019). Integration of persistent scatterer interferometry and ground data for landslide monitoring: the Pianello landslide (Bovino, Southern Italy). *Landslides*, 16(3): 447–468. DOI: https://doi.org/10.1007/S10346-018-01124-0/FIGURES/16.

Scaioni, M., Longoni, L., Melillo, V. & Papini, M. (2014). Remote Sensing for Landslide Investigations: An Overview of Recent Achievements and Perspectives. *Remote Sensing*, 6(10): 9600–9652. DOI: https://doi.org/10.3390/RS6109600.

Schuster, R.L. (1996). Socioeconomic significance of landslides. *Landslides: Investigation and mitigation*, 247: 12-35.

Solari, L., Raspini, F., Del Soldato, M., Bianchini, S., Ciampalini, A., Ferrigno, F., Tucci, S. & Casagli, N. (2018). Satellite radar data for back-analyzing a landslide event: the Ponzano (Central Italy) case study. *Landslides*, 15(4): 773–782. DOI: https://doi.org/10.1007/s10346-018-0952-x.

Strozzi, T., Luckman, A., Murray, T., Wegmüller, U. & Werner, C.L. (2002). Glacier motion estimation using SAR offset-tracking procedures. *IEEE Transactions on Geoscience and Remote Sensing*, 40(11): 2384–2391. DOI: https://doi.org/10.1109/TGRS.2002.805079.

Tarquini, S., Vinci, S., Favalli, M., Doumaz, F., Fornaciai, A. & Nannipieri, L. (2012). Release of a 10-m-resolution DEM for the Italian territory: Comparison with global-coverage DEMs and anaglyph-mode exploration via the web. *Computers & Geosciences*, 38(1): 168–170. DOI: https://doi.org/10.1016/J.CAGEO.2011.04.018.

Wang, C., Ge, D., Zhang, G., Zhu, W., Xiong, S., Liu, Y., Yang, H., Wang, S., Xu, L. & Peng, J. (2022). Monitoring and Stability Analysis of the Deformation in the Woda Landslide Area in Tibet, China by the DS-InSAR Method. *Remote Sensing*, 14(3): 532. DOI: https://doi.org/10.3390/RS14030532.

Wang, C., Mao, X. & Wang, Q. (2016). Landslide Displacement Monitoring by a Fully Polarimetric SAR Offset Tracking Method. Remote Sensing 8(8): 624. DOI: https://doi.org/10.3390/RS8080624.

Wasowski, J. & Bovenga, F. (2014). Investigating landslides and unstable slopes with satellite Multi Temporal Interferometry: Current issues and future perspectives. *Engineering Geology*, 174: 103–138. DOI: https://doi.org/10.1016/J.ENGGEO.2014.03.003.

Wegmüller, U., Werner, C., Strozzi, T. & Wiessman, A. (2002). Automated and Precise Image Registration Procedures. *Analysis of Multi-Temporal Remote Sensing Images*, 37–49. DOI: https://doi.org/10.1142/9789812777249_0002.

Zhao, C. & Lu, Z. (2018). Remote Sensing of Landslides—A Review. *Remote Sensing*, 10(2): 279. DOI: https://doi.org/10.3390/RS10020279.